Title
Evaluation of [11C]TAZA for amyloid β plaque imaging in postmortem human Alzheimer's disease brain region and whole body distribution in rodent PET/CT

Journal
Synapse, 70(4)

ISSN
0887-4476

Authors
Pan, Min-Liang
Mukherjee, Meenakshi T
Patel, Himika H
et al.

Publication Date
2016-04-01

DOI
10.1002/syn.21893

Peer reviewed

HHS Public Access

Author manuscript

Synapse. Author manuscript; available in PMC 2017 April 01.

Published in final edited form as:

Synapse. 2016 April ; 70(4): 163–176. doi:10.1002/syn.21893.

Evaluation of [^{11}C]TAZA for Amyloid β Plaque Imaging in Postmortem Human Alzheimer's Disease Brain Region and Whole Body Distribution in Rodent PET/CT

MIN-LIANG PAN, **MEENAKSHI T. MUKHERJEE**, **HIMIKA H. PATEL**, **BHAVIN PATEL**, **CRISTIAN C. CONSTANTINESCU**, **M. REZA MIRBOLOOKI**, **CHRISTOPHER LIANG**, and **JOGESHWAR MUKHERJEE***

Preclinical Imaging, Department of Radiological Sciences, University of California, Irvine, California 92697

Abstract

Objective—Alzheimer's disease (AD) is a neurodegenerative disease characterized by Aβ plaques in the brain. The aim of this study was to evaluate the effectiveness of a novel radiotracer, 4-[^{11}C]methylamino-4′-*N,N*-dimethylaminoazo-benzene ([^{11}C]TAZA), for binding to Aβ plaques in postmortem human brain (AD and normal control (NC)).

Methods—Radiosyntheses of [^{11}C]TAZA, related [^{11}C]Dalene (^{11}C-methylamino-4′-dimethylaminostyrylbenzene), and reference [^{11}C]PIB were carried out using [^{11}C]methyltriflate prepared from [^{11}C]CO_2 and purified using HPLC. In vitro binding affinities were carried out in human AD brain homogenate with Aβ plaques labeled with [^{3}H]PIB. In vitro autoradiography studies with the three radiotracers were performed on hippocampus of AD and NC brains. PET/CT studies were carried out in normal rats to study brain and whole body distribution.

Results—The three radiotracers were produced in high radiochemical yields (>40%) and had specific activities >37 GBq/μmol. TAZA had an affinity, K_i = 0.84 nM and was five times more potent than PIB. [^{11}C]TAZA bound specifically to Aβ plaques present in AD brains with gray matter to white matter ratios >20. [^{11}C]TAZA was displaced by PIB (>90%), suggesting similar binding site for [^{11}C]TAZA and [^{11}C]PIB. [^{11}C]TAZA exhibited slow kinetics of uptake in the rat brain and whole body images showed uptake in interscapular brown adipose tissue (IBAT). Binding in brain and IBAT were affected by preinjection of atomoxetine, a norepinephrine transporter blocker.

Conclusion—[^{11}C]TAZA exhibited high binding to Aβ plaques in human AD hippocampus. Rat brain kinetics was slow and peripheral binding to IBAT needs to be further evaluated.

Keywords

[^{11}C]TAZA; human Aβ plaque; Alzheimer's disease; PET imaging; norepinephrine transporter; brown adipose tissue

*Correspondence to: Jogesh Mukherjee; Medical Sciences B138, Department of Radiological Sciences, University of California, Irvine, Irvine, CA 92697-5000. j.mukherjee@uci.edu.

INTRODUCTION

Alzheimer's disease (AD) is the most common type of dementia, accounting for 50%–80% of dementia cases characterized by the accumulation of amyloid β (Aβ) plaques and neurofibrillary tangles (NFT) in the brain (Braak and Braak, 1991). Benzothiazole derivatives, such as [^{11}C]PIB (Fig. 1; **1**), have been developed to bind amyloid β (Aβ) plaques with high affinity and are capable of crossing the brain–blood barrier to be valuable for the application of in vivo Aβ plaque imaging in PET studies (Mathis *et al.*, 2003). Imaging with [^{11}C]PIB plays an essential role in the clinical studies for evaluation of drug efficacy in relation to the development of the Aβ plaques in vivo (Klunk *et al.*, 2004). As an Aβ plaque radiotracer, [^{11}C]PIB characteristic changes in the brains of patients with AD has played a major role in the AD neuroimaging initiative (e.g., Weiner *et al.* 2015). Efficacy of bapineuzumab, a humanized N-terminal specific anti-Aβ monoclonal antibody, in AD was conducted in a large multicentre phase 3 clinical trial and used [^{11}C]PIB for monitoring changes in Aβ plaques (Rinne *et al.*, 2010;Salloway *et al.*, 2014).

Following a large number of human research studies using [^{11}C]PIB in mild cognitive impairment (MCI) and AD (Raniga *et al.*, 2008; Weiner *et al.*, 2015), fluorinated [^{18}F]Florbetapir (Fig. 1; **2**) was the first fluorine-18 agent approved for clinical use in AD (Stephenson *et al.*, 2007; Zhang *et al.*, 2005; Zhu *et al.*, 2014). Although fluorine-18 offers advantages of the longer half-life, the wider use of [^{18}F]Florbetapir has been slow (Camus *et al.*, 2012). High white matter binding and the low standard uptake values (SUV) in the cortex of AD has caused caution. Thus, an agent that can provide a significantly higher SUV in the AD cortex may be an improvement toward clinical value. There has been continued interest in the development of Aβ plaque imaging agents that are labeled with fluorine-18 and which may provide a higher target to nontarget ratio (Cai *et al.*, 2007; Mathis *et al.*, 2012; Ni *et al.*, 2013; Verhoeff *et al.* 2008; Zhu *et al.*, 2014). Table I describes agents for imaging plaques some of which were recently approved by FDA, although there have been many more promising agents under development (Eckroat *et al.*, 2013; Tu *et al.*, 2015; Vandenberghe *et al.*, 2010). With increasing efforts to find treatments and cure for AD, there is much research into imaging plaques and NFT essential to the diagnosis and clinical management of AD (Ariza *et al.*, 2015; Barten and Albright, 2008; Schenk *et al.* 1999; Verhoeff, 2007; Zimmer *et al.*, 2014).

Congo red (Fig. 1; **3**) is a well-known dye which has also been used to assay amyloid aggregation (e.g., Jameson *et al.*, 2012). The unique "diazo" structure present in Congo red makes it different from the other known structures such as thioflavin and stilbenes from which PIB and Florbetapir were derived (Fig. 1; **1**,**2**). Iodinated phenyldiazenyl benzothiazole derivatives (Fig. 1; **4**) have recently been reported for imaging NFT in AD brains (Matsumura *et al.*, 2011). We have identified a unique compound, [^{11}C]TAZA [4-methylamino-4′-*N*,*N*-dimethylaminoazobenzene(Mukherjee *et al.*, 2012; Fig. 1; **5**)] as a radioligand for the binding site of Aβ plaque which has the "azo" functionality found in Congo red. It was anticipated that the structure of TAZA, with the additional "azo" heteroatoms (Fig. 1b, shown in green ovals, in structures **3**, **4,** and **5**) may render it less lipophilic toward white matter. [^{11}C]TAZA has the "aminomethylphenyl" structure (Fig. 1a, shown in red boxes, in structures **1**, **2**, **5,** and **6**). For purposes of comparison, we also

prepared [^{11}C]Dalene [4-methylamino-4′-*N*,*N*-dimethylaminostyrylbenzene; (Fig. 1; **6**; reported previously Kung *et al.*, 2003)], which instead of the "azo" moiety found in TAZA, contains the olefin. This olefin structure in Dalene is similar to that found in Florbetapir and also in its related analogue, Florbetaben (Villemagne *et al.*, 2011). The "dimethylaminophenyl" structure (Fig. 1c, shown in blue boxes, is in structures **4, 5,** and **6**).

In order to assess the value of [^{11}C]TAZA in Aβ plaque imaging, we report here the following: 1. Measurement of in vitro binding affinity of TAZA to human Aβ plaques; 2. Radiosynthesis of [^{11}C]TAZA, as well as the radiosynthesis of [^{11}C]Dalene for purposes of comparison using in vitro and in vivo studies with [^{11}C]PIB. 3. Comparison of the binding of the 3 radiotracers, [^{11}C]TAZA, [^{11}C]Dalene and [^{11}C]PIB to postmortem AD human brain slices. 4. Evaluation the three radiotracers, [^{11}C]TAZA, [^{11}C]Dalene and [^{11}C]PIB in normal rats in order to assess brain and whole body distribution of the radiotracers.

MATERIALS AND METHODS

General methods

All compressed gases including helium, hydrogen, and nitrogen with 0.25% oxygen were supplied by Airgas. A GE Scanditronix MC17 cyclotron (17 MeV, 45 μA) was used to generate high specific activity [^{11}C]CO_2 using a nitrogen gas target ([^{14}N] to [^{11}C] using p, α reaction). Carbon-11 radioactivity were counted in a Capintec CRC-15R dose calibrator while low level counting was carried out in a Capintec Caprac-R well-counter. Automated synthesizer, GE TRACERlab FX_{cPRO} (TRACERlab; from GE Healthcare, Milwaukee, WI) was used for all radiosyntheses. Shimalite-Ni by Shimadzu was applied as a catalyst for [^{11}C]CO_2 reduction. Molecular Sieves 4A, 80/100 mesh was from Alltech Ascarite, 20–30 mesh, silver triflate, iodine, and other chemicals were supplied by Aldrich-Sigma Corporation. Porapak Q 50–80 mesh was used for the [^{11}C]CH_3I trap and 60–80 mesh. Carbosphere was prepared for the silver triflate column. All solvents used were provided by Fisher Scientific. For quality control (QC) residual solvent gas chromatography with FID, a HP 6890 with 30 m Rtx 624 silica column was used. For QC chemical purity, a Waters or Gilson HPLC system with UV detector set at 350 nm was used with 4.6 × 250 mm C18 Econosil reverse-phase analytical column was used. A semipreparative HPLC column 100 × 250 mm 10 μm Econosil C18 reverse-phase was supplied by Grace Discovery Corp. for purification within the TRACER-lab. Millex-FG sterile pyrogen free 0.20 μm filters and Corning sterile filters were used as vent cartridges. Syringes were supplied by BD. The precursor, 2-(4′-aminophenyl)-6-hydroxybenzothiazole, and reference standard 2-(4′-methylaminophenyl)-6-hydroxybenzothiazole (PIB) were obtained from ABX, Germany and precursors, 4-amino-4′-(*N*,*N*-dimethylamino)stilbene (TCI America, Portland, OR) and 4-amino-4′-*N*,*N*-dimethylaminoazobenzene (Aldrich Chem Co., St. Louis, MO) were obtained commercially. Empty sterilized vials (10 mL), sterile water, saline USP were from Hospira Pharmaceuticals and ethanol 200 proof, USP (Pharmco-AAPER) were used for formulation. C-18 Sep Pak light cartridges were supplied by Waters Corp. for extraction.

Analytical thin-layer chromatography (TLC) was used to monitor reactions (Baker-flex, Phillipsburg, NJ). Electrospray mass spectra were obtained from a Model 7250 mass spectrometer (Micromass LCT). Proton NMR spectra were recorded on a Bruker OM EGA

500-MHz spectrometer. Tritium was assayed using a Packard Tri-Carb Liquid scintillation counter with 65% efficiency. Human postmortem brain tissue samples were obtained from the UCI Alzheimer's Disease Research Center (ADRC) brain tissue repository for in vitro experiments. Age and gender matched AD brain and normal control brain tissue (hippocampus; n =4) were used. AD brain samples selected for end-stage pathology (Braak & Braak stage of VI (Braak and Braak, 1991). Chunks of frozen tissue were dissected for immunohistochemical and autoradiographic techniques, as well as for biochemical experiments. Human postmortem brain slices were obtained on a Leica 1850 cryotome. Carbon-11 autoradiographic studies were carried out by exposing tissue samples on storage phosphor screens (Perkin Elmer Multisensitive, Medium MS). The apposed phosphor screens were read and analyzed by Opti-Quant acquisition and analysis program of the Cyclone Storage Phosphor System (Packard Instruments Co., Boston, MA). A preclinical Inveon dedicated PET scanner (Siemens Medical Solutions, Knoxville, TN) with a transaxial FWHM of 1.46 mm, and axial FWHM of 1.15 mm (Constantinescu and Mukherjee, 2009) was used for the PET studies. PET/CT images of rats were obtained and analyzed using ASIProVM, IRW, and PMOD softwares. All animal studies were approved by the Institutional Animal Care and Use Committee of University of California-Irvine. Postmortem human brain studies were approved by the Institutional Biosafety Committee of University of California, Irvine, CA.

In vitro binding affinity

Binding affinities of TAZA (prepared by reacting 4-amino-4′-dimethylaminoazobenzene with methyl triflate and purified by preparative TLC to provide TAZA (4-methylamino-4′-*N,N*-dimethylaminoazobenzene mass spectra (m/z, %), 255, $[M + H]^+$, 100%) and PIB were measured using human AD brain homogenate. Human brain homogenates were labeled with ^{3}H-PIB which is known to bind to human Aβ-amyloid. The brain tissue (hippocampal tissue from AD subject; 0.16 g) was homogenized in 10 mL of assay buffer for 30 s (10 mM PBS, pH 7.4) using Tekmar tissumizer (15 s, half maxima speed). A fixed concentration of [^{3}H]PIB (2 nM) was incubated with the brain homogenate in the presence of various concentrations of TAZA and PIB ($10^{-11–10\ -5}$M) in the assay buffer (10% ethanol, 90% 10 mM PBS, pH 7.4). Nonspecific binding was determined by including 10 μM of PIB. Total assay volume was 0.5 mL. To start, 0.2 mL of the brain homogenate was added to each test tube containing [^{3}H]PIB, different concentrations of drugs and 10 μM of PIB for nonspecific binding. The assay was done in duplicate and all test tube samples were incubated for 1 h in a 37°C water bath. After incubation a rapid vacuum filtration was implemented through Whatman GF/C filter article (pre-soaked in 0.1% polyethylamine in 10 mL of Millipore water) using Brandel tissue harvester. The filter was washed three times with 5 mL of cold buffer and was transferred to vials with 5 mL Bio-Safe II scintillation cocktail and counted for 10 min in a scintillation counter. Data were analyzed using following procedure: (a) the nonspecific binding of [^{3}H]PIB was subtracted for all samples; (b) the specific binding was normalized to 100% (no competitive ligand), and (c) the binding isotherms were fit to the Hill equation (KELL BioSoft software (v 6), Cambridge, U.K.). The K_i was calculated by the Cheng-Prussof equation using the reported kd[a] value, for ^{3}H-PIB.

Radiosynthesis

^{11}C-methyl triflate (^{11}C-methylating agent)—The [^{11}C]CO_2 (>37GBq) was produced in the MC-17 cyclotron and transferred to the TRACERlab automated radiosynthesis unit where the [^{11}C]CO_2 was trapped on the molecular sieve (0.3 g) in the packed column at T =25°C. Conversion to [^{11}C]methane ([^{11}C]CH_4) was achieved by reduction of [^{11}C]CO_2 with H_2 using 0.2 g Shimalite-Ni (Shimadzu) loaded on the molecular sieves (350°C for 30 s). Yields of [^{11}C]CH_4 averaged of 16–18 GBq. Gas-phase iodination of [^{11}C]CH_4 to [^{11}C]methyl iodide ([^{11}C]CH_3I) occurred at 760°C and iodine vessel at 90°C in a closed loop. The iodinated product, [^{11}C]CH_3I was passed over a MeI trap (Porapak Q, Alltech Corp.) with an average yield of [^{11}C]CH_3I of 16 GBq starting from >37GBq of [^{11}C]CO_2. The [^{11}C]CH_3I passed through the triflate column, which had been preheated to 195°C, and bubbled into the reaction vessel. The total automated reaction from [^{11}C]CO_2 to [^{11}C]methyl triflate ([^{11}C]CH_3OTf) was approximately 11 min and provided approximately 11 GBq of [^{11}C]CH_3OTf.

[^{11}C]TAZA—Radiosynthesis of [^{11}C]TAZA was carried out by reacting 4-amino-4′-dimethylaminoazobenzene (1 mg/0.5 mL acetone) with [^{11}C]CH_3OTf prepared in the TRACERlab. ^{11}C-Methyltriflate was trapped at −20°C in acetone containing the precursor and subsequently heated for 5 min at 80°C under helium gas atmosphere in a closed reaction vessel. This mixture was very bright yellow-red in color (due to the color of the precursor). Reverse phase HPLC purification (40:60 of 0.1% aqueous trimethylamine/acetonitrile, flow rate of 2.5 mL/min) provided [^{11}C]TAZA as the major radioactive product eluting at approximately 20 min. Purified [^{11}C]TAZA was taken up in 10% ethanol-90% sterile saline and filtered through a sterilizing filter into a sterile pyrogen-free single dose vial to provide approximately 500 MBq of [^{11}C]TAZA for in vitro and in vivo studies. Radiochemical purity was >95% and specific activity of [^{11}C]TAZA was >37 TBq/mmol.

[^{11}C]Dalene—Similar to the procedure outlined above in [^{11}C]TAZA section, radiosynthesis of [^{11}C]Dalene was carried out by reacting 4-amino-4′-dimethylaminostyrylbenzene (1 mg/0.5 mL acetone) with [^{11}C]CH_3OTf prepared in the TRACERlab. This mixture was very yellow in colour (due to the colour of the precursor, albeit less intense than TAZA). Reverse phase HPLC purification (40:60 of 0.1% aqueous trimethylamine/acetonitrile, flow rate of 1.5 mL/min) provided [^{11}C]Dalene as the major radioactive product eluting at approximately 40 min. Purified [^{11}C]Dalene was taken up in 10% ethanol-90% sterile saline and filtered through a sterilizing filter into a sterile pyrogen-free single dose vial to provide approximately 370 MBq of [^{11}C]Dalene for in vitro and in vivo studies. Radiochemical purity was >95% and specific activity of [^{11}C]Dalene was >37 TBq/mmol.

[^{11}C]PIB—Similar to the procedure outlined above in [^{11}C]TAZA section, radiosynthesis of [^{11}C]PIB was carried out by reacting 5-OH-BTA-0 (1 mg/0.5 mL acetone) with [^{11}C]CH_3OTf prepared in the TRACER-lab. Reverse phase HPLC purification (40:60 of aceto-nitrile/0.1 M ammonium formate, flow rate of 1 mL/min) provided [^{11}C]PIB as the major radioactive product eluting at approximately 8 min. The HPLC fraction was collected and diluted with 70 mL of MilliQ water, and isolated by solid phase extraction to a <10%

ethanolic isotonic saline solution which is filtered through a sterilizing filter into a sterile vial provided approximately 740 MBq of [^{11}C]PIB for in vitro and in vivo studies. Radiochemical purity was >95% and specific activity of [^{11}C]PIB was >37 TBq/mmol.

Postmortem human brain autoradiography

[^{11}C]TAZA, [^{11}C]PIB and [^{11}C]Dalene were used for autoradiographic studies. Human hippocampus sections (7 μm thick) were preincubated in buffer (40% EtOH) for 10 min. The brain sections were placed in a glass chamber and incubated with [^{11}C]TAZA, [^{11}C]PIB, and [^{11}C]Dalene (approximately 740 kBq/cc) in 40% EtOH at 37°C for 1 h. The slices were then washed with cold Millipore water, 70%–90%–70% EtOH, water for 2,1,1,1,1 min, respectively. Nonspecific binding was measured in the presence of 10 μM PIB. The brain sections were air-dried, exposed overnight on a phosphor film, and then placed on the Phosphor Autoradiographic Imaging System (Packard Instruments Co). Regions of interest (ROIs) were drawn on the slices and the extent of binding of ^{11}C-PIB was measured with DLU/mm^2 using the Opti-Quant acquisition and analysis program (Packard Instruments Co). Neighboring slices were immunostained with 4G8 antibody using modifications of reported methods (Braak *et al.*, 2011). Slides were warmed to room temperature and washed in TBS (Tris-buffered saline, pH 7.5), followed by antigen ret-rival in 70% formic acid for 15 min. After endogenous peroxidase quenching, sections were stained with bio-tinylated anti-Aβ antibody 4G8 (Covance, Princeton, NJ) at 1:800 dilution followed by incubation according to manufacturer instructions (Vector Labs, Burlingame, CA). Peroxidase reaction was developed with 3,3′-diaminobenzidine reagent (Vector Labs, Burlingame, CA). Pictures were taken on Olympus BX61 microscope.

In vivo rat PET/CT

Male Sprague-Dawley rats (308–468 g) were single housed in a climate controlled room and had full access to food and water. The rats were fasted 24 h prior to time of scan. On the day of the study, rats were anesthetized using 4.0% isoflurane. The rat was then positioned on the scanner bed by placing it on a warm-water circulating heating pad and kept anesthetized with 2.5% isoflurane anesthesia applied using a nose-cone. Preparation of dose injection was as follows: approximately 100 ± 25 MBq of [^{11}C]TAZA, [^{11}C]Dalene, or [^{11}C]PIB was drawn into a 0.5 mL syringe with a 29 gauge needle and diluted with sterile saline to a final volume of 0.3 mL. Rats received two 90 min scans on two separate days (1–4 weeks apart) with an Inveon dedicated PET scanner (Siemens Medical Solutions). On first day each rat received a baseline scan, one with [^{11}C]Dalene and the other with [^{11}C]TAZA. The second day each animal was preinjected iv with a 50 μL bolus of atomoxetine (ATX [1–2 mg/kg], 17 min before [^{11}C]Dalene and 2 min before [^{11}C]TAZA. Following PET each animal received a CT scan with an Inveon MM CT, which was used for attenuation and scatter correction. The CT scan was performed at 2 overlapping bed positions with detector-source rotating 220 degrees around the animal with 120 projections acquired. CT images were reconstructed with a cone beam algorithm into 480 × 480 × 632 image arrays with a 206 μm pixel size. All PET images were corrected for scatter, attenuation, and radioactive decay. Acquired list-mode were sorted dynamically into multiple frames. Image reconstruction was performed with an OSEM3D/fast MAP algorithm (16 OSEM 3D subsets, 2 iterations, 18 MAP iterations) resulting in 128 × 128 × 159 image array with a 0.79 mm pixel size. Images

were visualized and analyzed with ASIPro (CTI Concorde Microsystems, LLC.) and PMOD (PMOD Technologies) software.

Image analysis

Analysis was performed with PMOD software package (PMOD Technologies). All images were normalized to Paxinos & Watson space via coregistration with an MR rat template (Schweinhardt *et al.* 2003). Volumes of interest (VOIs) were drawn on the MR template and placed on brainstem, frontal cortex, cerebellum and other brain regions. VOIs of the inter-scapular BAT (IBAT) were delineated visually by contouring the uptake that was clearly above normal background uptake. VOIs from all regions were used to derive time-activity curves (TACs) and were normalized by dividing them the injected dose.

RESULTS

In vitro binding affinity studies

In vitro binding affinity of TAZA (Fig. 2) in human AD brain homogenates using [^{3}H]PIB yielded an IC_{50} of 1.28 nM for TAZA compared with 10 nM for PIB. These IC_{50} values for PIB are lower compared with previously reported values for PIB in AD brain homogenates of frontal cortex, IC_{50} of 3.84 nM (Hellstrom-Lindahl *et al.*, 2014). Inhibition constants were calculated using the Cheng-Prusoff equation ($K_i = IC_{50}/(1+(\text{conc of } [^{3}H]PIB)/kDa)$) and a kd[a]= 3.77 nM for [^{3}H]PIB (Fodero-Tavoletti *et al.*, 2007). The inhibition constant, K_i for TAZA was 0.84 nM and that for PIB was 6.67 nM. The measured K_i value for PIB is in the range of previously reported K_i values for PIB (Klunk *et al.*, 2004).

Radiosynthesis

Radiolabeling reactions used [^{11}C]CH_3OTf produced in the TRACERlab. Both [^{11}C]TAZA and [^{11}C]Dalene were the single major radiochemical product. Both the radiotracers were produced in high radiochemical yields and specific activity. The slower HPLC flow rate in the case of [^{11}C]Dalene increased the retention time but minimized the potential contamination from the starting material due to tailing of the starting material. It should be noted that the HPLC purification of [^{11}C]TAZA and [^{11}C]Dalene were carried out on a separate HPLC outside the TRACERlab unlike that of [^{11}C]PIB which was done using the in-built HPLC in TRACERlab. The three radiotracers were prepared in amounts of 370–740 MBq in specific activities generally >37 TBq/mmol and were found to be stable in 10% ethanolic saline solution for in vitro and in vivo studies.

Postmortem human AD brain autoradiography

Extensive binding of [^{11}C]TAZA was seen in the gray matter regions of the two AD subjects as seen in Figures 3B and 3F while white matter had significantly lower binding. This gray matter binding was significantly reduced when the brain sections were treated with PIB (Fig. 3C). The binding in the gray matter was confirmed by immunostaining for the presence of Aβ plaques as can be seen in Figures 3D and 3G. Normal control subjects had very little gray matter binding compared with the AD subjects (Figs. 3H and 3I). As can be seen in Figure 3J, AD2 subject had the greatest amount of [^{11}C]TAZA binding followed by AD1 subject. The NC1 subject had little [^{11}C]TAZA binding while NC2 exhibited some localized

hot spots. Over 90% of the binding of [^{11}C]TAZA was displaced by PIB from the AD1 and AD2 subjects.

Shown in Figure 4 is a comparison of the degree of binding of [^{11}C]TAZA, [^{11}C]Dalene and [^{11}C]PIB in AD2 and NC1 subjects. The highest amount of gray matter binding was observed with [^{11}C]TAZA and the highest amount of white matter binding was observed with [^{11}C]Dalene. The three radiotracers exhibited little binding in the normal control subjects, although [^{11}C]Dalene exhibited higher nonspecific binding (Fig. 4D) compared with [^{11}C]TAZA and [^{11}C]PIB. The gray matter to white matter ratio (GM/WM) was the greatest for [^{11}C]TAZA as shown in Table II. The ratio of 19.6 for AD1 and 30.5 for AD2 was due to both the high binding in GM and low binding in WM for [^{11}C]TAZA as can be seen in Figure 4G. Lowest ratios (approximately 5-fold lower than [^{11}C]TAZA) were measured for [^{11}C]Dalene due to the higher WM binding. The GM/WM ratios of [^{11}C]PIB were higher than [^{11}C]Dalene, but about 4-fold lower than [^{11}C]TAZA (Table II).

PET/CT studies

Rat brain uptake of [^{11}C]TAZA after intravenous administration occurred slowly over the 90 min PET scan (Figs. 5A–5C). Regional brain localization of [^{11}C]TAZA was confirmed by coregistering the PET scan with a rat brain MRI template (Fig. 5A). Greatest uptake of [^{11}C]TAZA occurred in the brainstem followed by cerebellum and the frontal cortex (Fig. 5B). Uptake of [^{11}C]TAZA plateaued at approximately 60 min. The maximum activity levels in the various brain regions reached approximately 0.3% injected dose/cc. Ratios of brainstem to frontal cortex was 1.78 at 85 min while cerebellum to frontal cortex was 1.20, respectively.

A similar slow brain uptake over the 90 min scan was observed for [^{11}C]Dalene (Figs. 5D–5F). Regional brain localization of [^{11}C]Dalene was similar to [^{11}C]TAZA, which was confirmed by coregistering the PET scan with the rat brain MRI template (Fig. 5D). [^{11}C]Dalene distribution was observed in the brainstem which was a little more discrete compared with [^{11}C]TAZA, followed by cerebellum and the frontal cortex (Fig. 5E). Uptake of [^{11}C]Dalene appeared to plateau at approximately 60 min. The peak levels in the various brain regions were lower than those measured for [^{11}C]TAZA reaching approximately 0.1% injected dose/cc. Ratios of brainstem and cerebellum to frontal cortex at 85 min were 1.80 and 1.04, respectively.

Whole body PET/CT scans with [^{11}C]TAZA and [^{11}C]Dalene revealed distinct distribution features and similarities between the two radiotracers (Fig. 6). Localization of [^{11}C]Dalene was visualized in interscapular brown adipose tissue (IBAT) and confirmed with the coregistered PET/CT scan (Fig. 6A). Uptake of [^{11}C]Dalene in IBAT was gradual and similar to that observed in the brainstem. Activity in IBAT leveled off sooner (approximately 20 min) than was observed in the brain to a similar level of 0.12% injected dose/cc (Fig. 6C). Compared with [^{11}C]Dalene, higher levels of [^{11}C]TAZA binding was observed in IBAT (Fig. 6B). In addition to IBAT, other regions of brown adipose tissue (BAT) were also observed (Fig. 6B) consistent with our previous studies on activated BAT in the rat (Mirbolooki *et al.*, 2011). Uptake of [^{11}C]TAZA in IBAT was gradual and continued to

increase beyond the scan time of 90 min with 0.43% injected dose/cc at the end of the scan. This uptake was greater than [^{11}C]TAZA measured in the brain regions.

MicroPET/CT atomoxetine competition studies

Our previous [^{18}F]FDG studies with atomoxetine, a norepinephrine transporter (NET) inhibitor have shown a high level of activation of IBAT as well as other BAT areas in the rodent model (Mirbolooki *et al.*, 2013), similar to the accumulation of [^{11}C]TAZA seen in Figure 6B. The activation occurred by elevated levels of norepinephrine due to the blocking of NET by atomoxetine in the sympathetic innervation in BAT regions. In order to assess the potential interaction of [^{11}C]TAZA at the NET sites in BAT, competition studies with atomoxetine were carried out. Preinjection of atomoxetine prior to administration of [^{11}C]TAZA had a major effect on BAT binding of [^{11}C]TAZA (Figs. 7A and 7B). Binding of [^{11}C]TAZA was reduced in all areas of BAT as seen in Figure 7B and time-activity curves shown in Figure 7C show a very different uptake and clearance in the presence of atomoxetine. Atomoxetine caused a rapid high initial uptake (0.15% injected dose/cc) followed by a clearance of [^{11}C]TAZA from IBAT to 0.02% injected dose/cc. This suggests a competitive inhibition of [^{11}C]TAZA by atomoxetine in BAT regions. The time-activity curve of [^{11}C]TAZA in the presence of atomoxetine resembled the uptake and clearance curve of [^{11}C]PIB in IBAT (Fig. 7C).

Brain uptake of [^{11}C]TAZA in the presence of atomoxetine was dramatically different compared with the baseline scans (Fig. 7D). Initial brain uptake was very high (up to 1% injected dose/cc in the brainstem) which cleared rapidly over the duration of the 90 min from all brain regions. Like the baseline study, greater uptake of [^{11}C]TAZA occurred in the brainstem followed by cerebellum and the frontal cortex (Fig. 7D). The minimal activity levels in the brainstem went down to approximately 0.24% injected dose/cc while the activity levels in the frontal cortex were similar to the maximal levels in the baseline study (Table III). Ratio of brainstem to frontal cortex was 1.58 at 85 min while cerebellum to frontal cortex was 1.10.

Preinjection of atomoxetine prior to administration of [^{11}C]Dalene had a similar effect on BAT binding of [^{11}C]Dalene (Fig. 7E). [^{11}C]Dalene was reduced in IBAT and time-activity curves shown in Figure 7E show a very different uptake and clearance in the presence of atomoxetine. Atomoxetine caused a rapid high initial uptake (0.05% injected dose/cc) followed by a slow clearance of [^{11}C]Dalene from IBAT to 0.05% injected dose/cc rather than a rise as seen in the baseline scan. This suggests a competitive inhibition of [^{11}C]Dalene by atomoxetine in BAT regions. The clearance in the time-activity curve of [^{11}C]Dalene in the presence of atomoxetine was not as rapid as seen in the case of [^{11}C]TAZA (Fig. 7C).

Like [^{11}C]TAZA, brain uptake of [^{11}C]Dalene in the presence of atomoxetine was dramatically different compared with the baseline scans (Fig. 7F). Initial brain uptake was very high (up to 1.1% injected dose/cc in the brainstem) which cleared rapidly over the duration of the 90 min from all brain regions. Like the baseline study, greater uptake of [^{11}C]Dalene occurred in the brainstem followed by cerebellum and the frontal cortex (Fig. 7F). The minimal activity levels in the brainstem went down to approximately 0.53%

injected dose/cc while the activity levels in the frontal cortex were a little lower (0.30% injected dose/cc) (Table III). Ratio of brainstem to frontal cortex was 1.75 at 85 min while cerebellum to frontal cortex was 1.0.

DISCUSSION

Several amyloid plaque imaging agents continue to be developed in an effort to obtain new agents with high affinity for the amyloid plaques and lower non-specific binding (Eckroat *et al.*, 2013). The outcome of such efforts is to translate to higher in vivo SUV values, thus making measurement of changes between NC, mild cognitive impairment (MCI) and AD more precise. Currently, there are at least four imaging agents in use for human Aβ amyloid plaques, in addition to [^{11}C]PIB which continues to be the standard of reference. Table I summarizes some of these agents and their relative binding affinities with respect to PIB. The four fluorinated agents florbetaben, florbetapir, flutemeatmol, and NAV4,694 had relative binding of 0.4, 0.3, 1.1, and 0.4, respectively, with respect to PIB, suggesting that only flutemetamol has a slightly higher affinity than PIB (0.74 nM vs. 0.80 nM, Choi *et al.*, 2009). The affinity of TAZA was found to be approximately 5 times higher than PIB, suggesting a significant effect of the “azo” functionality on the binding to Aβ plaques. Dalene, the analogue of TAZA without the “azo” linker had a weaker affinity (15 nM measured using ^{125}I-TZDM, Kung *et al.*, 2003) and was found to be about 5 times weaker compared to the related compound SB-13 (Kung *et al.*, 2003). The significant effect of the “azo” linker was also confirmed by phenyldiazenyl benzothiazoles, which were found to be markedly more potent than SB-13 (Matsumura *et al.*, 2011). Thus, it appeared that TAZA has a higher affinity for Aβ amyloid plaques and worthy of further *in vitro* and in vivo evaluation. It must be noted that phenyldiazenyl benzothiazoles (PDB derivatives) were also found to have a high affinity for tau aggregates (Matsumura *et al.*, 2011; Tau =0.48 nM and $A\beta_{1-42}$ = 8.24 nM for PDB-3, Fig. 1).

Since TAZA contained three *N*-methyl groups, radiolabeling with carbon-11 methyl group of the precursor in a single step without the need of any protecting group was the easiest option. Carbon-11 methylation has been carried out resulting in high radiochemical purity and specific activity of various radiotracers (e.g., Mukherjee *et al.*, 2004; Shao *et al.*, 2011; Wilson *et al.*, 2004). The use of [^{11}C]methyl triflate as a more reactive methylating agent was used for radiolabeling of [^{11}C]SB-13 (Ono *et al.*, 2003). The TRACERlab was designed to use either [^{11}C]CH_3I or [^{11}C]CH_3OTf for carrying out [^{11}C]methylations in a routine, automated manner for multiple [^{11}C]radiolabeled compounds, including [^{11}C]PIB (Shao *et al.*, 2011; Wilson *et al.*, 2004). Since both [^{11}C]TAZA and [^{11}C]Dalene are chemically related structures to [^{11}C]SB-13 and [^{11}C]PIB, radiolabeling was efficiently carried out using [^{11}C]CH_3OTf in the TRACERlab. Product purification using an inbuilt HPLC system, a solid-liquid phase extraction through C18-filter cartridge, and continuing to dose formulation through a 0.2 μm sterile pyrogen-free filter was used in the automated radiosynthesis of [^{11}C]PIB in the TRAC-ERlab. For [^{11}C]TAZA and [^{11}C]Dalene, we used the reaction vial for the radiolabeling reaction, but purification and dose formulation was carried out in a separate HPLC outside the TRACERlab. The “HPLC loop” method (Ono *et al.*, 2003) may serve well in reducing the amount of precursor material needed (and help reduce the amount of highly chromophoric precursors in the HPLC purification).

High levels of [^{11}C]TAZA binding were found in the AD hippocampus gray matter regions. The levels of binding were greater for AD subject #2 and correlated with the immunostained Aβ amyloid plaques. White matter had very low, background levels and were similar to those found in the normal control subjects. [^{11}C]TAZA This binding was dramatically reduced (>94%) in the presence of PIB suggesting that binding of [^{11}C]TAZA occurred predominantly at the similar site as PIB. Since [^{11}C]PIB binds to Aβ amyloid plaques and not to NFT (Klunk *et al.*, 2004), our findings suggests that [^{11}C]TAZA binding in the AD hippocampus is to Aβ amyloid plaques. These observations also suggest that the "benzothiazole moiety" present in the PDB derivatives may be contributing to their affinity to NFT (Matsumura *et al.*, 2011). Further studies with [^{11}C]TAZA are required to establish the selectivity to Aβ amyloid plaques.

Comparing the binding of the three radiotracers, [^{11}C]TAZA had the highest gray matter to white matter ratios in both AD subjects. The extent of binding in AD2 was greater than AD1, although both were at a similar Aβ amyloid plaque stage (Table II). The differences may be due to the size and location of the hippocampal tissue between the two AD subjects. The normal controls had little binding, although local hot spots were visible in normal control 1. Binding of [^{11}C]PIB was about 4-fold lower than [^{11}C]TAZA in both the AD subjects when the gray matter to white matter ratios were compared. Lowest ratios were found for [^{11}C]Dalene with [^{11}C]PIB showing a 1.4-fold greater ratio compared with [^{11}C]Dalene. The pattern of binding in the two AD subjects was similar for the three radiotracers. Although in vitro ratios do not directly translate to in vivo measures, these findings suggest that [^{11}C]TAZA may be expected to give a significantly higher uptake compared with [^{11}C]PIB in PET studies of AD subjects.

In vivo PET studies were carried out in healthy rats with the three radiotracers. The uptake of the radiotracers was highest in the brainstem region followed by frontal cortex and cerebellum. Midbrain also had some scattered binding. Brain uptake of both, [^{11}C]TAZA and [^{11}C]Dalene was low as can be seen in Figure 5C,F in all brain regions. This is in contrast to [^{11}C]PIB which rapidly enters the brain. The initial uptake of the three radiotracers, [^{11}C]TAZA, [^{11}C]Dalene and [^{11}C]PIB at 4.5 min post-intravenous injection in the frontal cortex were 0.007, 0.015, and 0.714% injected dose/cc, respectively while at 85 min postinjection they were 0.16, 0.069, and 0.045% injected dose/cc (Table III). The early-to-later PET ratio for [^{11}C]PIB in the frontal cortex was >15, while [^{11}C]TAZA and [^{11}C]Dalene were below unity. This high ratio for [^{11}C]PIB is consistent with previously reported kinetics in mice brains (Mathis *et al.*, 2012). Ratio of brainstem to frontal cortex at 85 min postinjection was 1.78 for [^{11}C]TAZA, 1.80 for [^{11}C]Dalene, and 1.24 for [^{11}C]PIB, suggesting greater brainstem binding of [^{11}C]TAZA and [^{11}C]Dalene compared with [^{11}C]PIB. Delivery of the two radiotracers, [^{11}C]TAZA and [^{11}C]Dalene to the brain appears to be limited in the various brain regions, but at later time points resembles the levels found with [^{11}C]PIB. Brain levels appear to plateau at approximately 60 min postinjection (Figs. 5C and 5F). Similar slow brain uptake has been reported for the related "azo" derivative **4**, ^{125}I-PDB in mice with levels in the mice brain going from 0.94%injected dose/organ at 2 min to 2.89%injected dose/organ at 60 min postinjection (Matsumura *et al.*, 2011). In a recent study, ^{13}N-labeled azo benzenesulfonic acid derivatives were evaluated in transgenic

mice (Tg 2576) and the derivative containing the synthon *b* and *c* in [^{11}C]TAZA (Fig. 1) showed promise in binding to Aβ plaques, both in vitro and in vivo (Gaja *et al.*, 2014).

Whole body PET/CT studies of the rats revealed significant binding of [^{11}C]TAZA and [^{11}C]Dalene in regions consistent with BAT (Figs. 6A and 6B). The uptake curves of the two radiotracers in the IBAT followed a similar, slow uptake, with [^{11}C]TAZA showing higher levels compared with [^{11}C]Dalene. For [^{11}C]TAZA, the levels were higher than the brainstem while [^{11}C]Dalene IBAT levels were similar to brainstem (Table III). Our previous findings with adrenergic pathway activation of BAT has revealed the innervation in interscapular BAT (IBAT), cervical BAT, periaortic BAT and intercostal BAT using β3 adrenoceptor agonist (Mirbolooki *et al.*, 2011) and NET inhibitor atomoxetine (Mirbolooki *et al.*, 2013). Localization of [^{11}C]TAZA was clearly visualized in IBAT, cervical BAT and periaortic BAT as seen in Figure 6B. Such consistent localization of [^{11}C]TAZA in BAT regions may be suggestive of a specific interaction with a molecular target in BAT. It should be noted that [^{11}C]PIB exhibited rapid uptake and clearance from IBAT with levels similar to the brainstem (Table III).

Previous reports have revealed micromolar affinities for NET uptake of stilbene and *N,N*-dimethylaminophenyldiazenyl derivatives containing the guanidino group (Hadrich *et al.*, 1999) and stilbene dimers (Smith *et al.*, 2012). NET existence in BAT has been reported in both rodents (Okuyama *et al.* 2002) and humans (Hadi *et al.* 2007). NET inhibitors such as atomoxetine play an important role in BAT activity by increasing norepinephrine levels verified by ^{18}F-FDG PET (Mirbolooki *et al.*, 2013). Based on these observations, we anticipated that the IBAT uptake of both [^{11}C]TAZA and [^{11}C]Dalene may be mediated by NET. Thus, we carried out preinjection experiments with atomoxetine on both [^{11}C]TAZA and [^{11}C]Dalene with the expectation of decreasing the binding of both [^{11}C]TAZA and [^{11}C]Dalene. Figure 7B shows significant decrease of [^{11}C]TAZA in BAT regions and the time-activity curve shown in Figure 7C exhibited a major change and rapid clearance which mimicked the curve for [^{11}C]PIB. Similar change in time-activity curve for [^{11}C]Dalene was seen with atomoxetine as seen in Figure 7F.

Brain NET are responsible for norepinephrine reuptake. NET has been shown to be involved in various psychiatric and behavioral disorders, such as attention deficit hyperactivity disorder (ADHD) (Bymaster *et al.*, 2002, Spencer *et al.*, 2002), substance abuse and depression (Klimek *et al.*, 1997), and AD (Herrmann *et al.*, 2004). NET imaging with PET is challenged due to the widespread distribution of NET in the brain and the lower contrast in density between NET-poor and NET-rich regions (Smith *et al.*, 2006). Of the tracers developed so far [^{11}C]MRB has shown improved specific binding (Gallezot *et al.* 2011; Logan *et al.*, 2007). [^{11}C]Dalene and [^{11}C]TAZA binding pattern (brainstem. thalamus, midbrain) appeared consistent with the expected NET distribution in the rat brain. [^{11}C]Dalene binding values were higher than those of [^{11}C]TAZA. Atomoxetine preinjection promoted a large and fast increase in [^{11}C]Dalene and [^{11}C]TAZA brain uptake. This effect could be attributed to systemic effects, such as changes in tracer free fraction and effects on blood flow. For [^{11}C]TAZA, interestingly, the ratio between the initial time (4.5 min postinjection) and later time (85 min postinjection) approached 5 for brain regions and in the case of IBAT it was 9 (Table III).

Although, our findings cannot be considered evidence that the secondary binding sites of these two tracers are on NET, changes in their accumulation in different regions in the presence of atomoxetine needs further evaluation, such as possible involvement of energy dependent Uptake-1 process or by diffusion, energy independent Uptake-2 process (Streby *et al.*, 2015). Brain levels of [^{11}C]TAZA in the presence of atomoxetine were significantly higher initially compared with baseline scans (without atomoxetine; Table III). At the end of the scan, the brainstem to frontal cortex ratio was only reduced by approximately 10% (from 1.78 to 1.58). This may suggest low "specific" binding to target NET regions in the normal brain. Similarly, autoradiographic studies in the normal human control hippocampus did not exhibit significant binding of [^{11}C]TAZA. However, further studies are needed to fully characterize the large effect of atomoxetine on the brain uptake of [^{11}C]TAZA in the rodent brain and identify species differences in the binding of [^{11}C]TAZA to NET. These studies will include deciphering the possible uptake (active transport via NET) of [^{11}C]TAZA into the NET presynaptic terminal.

In summary [^{11}C]TAZA presents the following features: (1) Increased signal to noise ratio. [^{11}C]TAZA has higher binding to the human Aβ-plaques compared with [^{11}C]PIB. The unique azo structure of TAZA results in a higher binding affinity for the human Aβ-plaques compared with PIB thus contributing to the higher binding of [^{11}C]TAZA. The increased signal to noise ratio may enhance sensitivity of detection of change in PET studies. (2) Decreased white matter binding. A lower amount of white matter binding was seen with [^{11}C]TAZA due to the heteroatoms in the "azo" functionality. This difference between gray matter and white matter may improve earlier delineation of AD, MCI and normal controls. (3) Enable transgenic animal imaging. Transgenic mouse models of AD have been shown to present strong, distinct pathologies of specific aspects of the human disease. Feasibility of imaging animal models with [^{11}C]TAZA will be useful for the development of therapeutic drugs and understanding AD (e.g., Gaja *et al.*, 2014; Snellman *et al.*, 2013).

Acknowledgments

We like to thank Alisha Bajwa for technical assistance with the binding affinity studies. We like to thank Dr. Vitaly Vasilevko for technical assistance with immunostaining and the UCI ADRC for the human brain tissue. Conflict of interest: the authors have no conflict of interest in the work reported here. Role of authors: All authors had full access to all the data in the study and take responsibility for the integrity of the data and the accuracy of the data analysis. Study concept and design: JM. Acquisition of data: MLP, MTM, HHP, BP, RM, CL. Analysis and interpretation of data: MLP, MTM, HHP, CC, RM. Drafting of the manuscript: MLP, JM, HHP, CC. Statistical analysis: JM, HHP, CC, RM. Obtained funding: JM. Study supervision: JM.

Contract grant sponsor: NIH/NIA AG 029479 (JM).

References

Ariza M, Kolb HC, Moechars D, Rombouts F, Andres JI. Tau positron emission tomography (PET) imaging: Past, present, and future. J Med Chem. 2015; 58:4365–4382. [PubMed: 25671691]

Barten DM, Albright CF. Therapeutic strategies for Alzheimer's disease. Mol Neurobiol. 2008; 37:171–186. [PubMed: 18581273]

Braak H, Braak E. Neuropathological staging of Alzheimer-related changes. Acta Neuropathol. 1991; 82:239–259. [PubMed: 1759558]

Braak H, Thal DR, Ghebremedhin E, Tredici KD. Stages of the pathologic process in Alzheimer's disease age categories from 1 to 100 years. J Neuropathol Exp Neurol. 2011; 70:960–969. [PubMed: 22002422]

Bymaster FP, Katner JS, Nelson DL, Hemrick-Luecke SK, Threlkeld PG, Heiligenstein JH, Morin SM, Gehlert DR, Perry KW. Atomoxetine increases extracellular levels of norepinephrine and dopamine in prefrontal cortex of rat: A potential mechanism for efficacy in attentiondeficit/hyperactivity disorder. Neuropsychopharm. 2002; 27:699–711.

Cai L, Innis RB, Pike VW. Radioligand development for PET imaging of b-amyloid (Ab)- current status. Curr Med Chem. 2007; 14:19–52. [PubMed: 17266566]

Camus V, Payoux P, Barre L, Desgranges B, Voisin T, Tauber C, La Joie R, Tafani M, Hommet C, Chetelat G, Mondon K, de La Sayette V, Cottier JP, Beaufils E, Ribeiro MJ, Gissot V, Vierron E, Vercouillie J, Vellas B, Eustache F, Guilloteau D. Using PET with 18F-AV-45 (florbetapir) to quantify amyloid load in a clinical environment. Eur J Nucl Med Mol Imag. 2012; 39:621–631.

Choi SR, Golding G, Zhuang Z, Zhang W, Lim N, Hefti F, Benedum TE, Kilbourn MR, Skovronsky D, Kung HF. Preclinical properties of 18F-AV-45: A PET agent for Abeta plaques in the brain. J Nucl Med. 2009; 50:1887–1894. [PubMed: 19837759]

Constantinescu C, Mukherjee J. Performance evaluation of an Inveon PET preclinical scanner. Phys Med Biol. 2009; 54:2885–2899. [PubMed: 19384008]

Eckroat TJ, Mayhoub AS, Garneau-Tsodikova S. Amyloid-β probes: Review of structure-activity and brain-kinetics relationships. Beilstein J Org Chem. 2013; 9:1012–1044. [PubMed: 23766818]

Fodero-Tavoletti MT, Smith DP, McLean CA, Adlard PA, Barnham KJ, Foster LE, Leone L, Perez K, Cortes M, Culvenor JG, Li QX, Laughton KM, Rowe CC, Masters CI, Cappai R, Villemagne VL. In vitro characterization of Pittsburgh compound-B binding to Lewy bodies. J Neurosci. 2007; 27:10365–10371. [PubMed: 17898208]

Gaja V, Gomez-Vallejo V, Puigivila M, Perez-Campana C, Martin A, Garcia-Osta A, Calvo-Fernandez T, Cuadrado M, Franco R, Lliop J. Synthesis and evaluation of ^{13}N-labelled azo compounds for b-amyloid imaging in mice. Mol Imag Biol. 2014; 16:538–549.

Gallezot JD, Weinzimmer D, Nabulsi N, Lin SF, Fowles K, Sandiego C, McCarthy TJ, Maguire RP, Carson RE, Ding YS. Evaluation of [(11)C]MRB for assessment of occupancy of norepinephrine transporters: Studies with atomoxetine in non-human primates. Neuroimage. 2011; 56:268–279. [PubMed: 20869448]

Hadi M, Chen CC, Whatley M, Pacak K, Carrasquillo JA. Brown fat imaging with (18)F-6-fluorodopamine PET/CT, (18)F-FDG PET/CT, and (123)I-MIBG SPECT: A study of patients being evaluated for pheochromocytoma. J Nucl Med. 2007; 48:1077–1083. [PubMed: 17574980]

Hadrich D, Berthold F, Steckhan E, Bonisch H. Synthesis and characterization of fluorescent ligands for the norepinephrine transporter: Potential neuroblastoma imaging agents. J Med Chem. 1999; 42:3101–3108. [PubMed: 10447954]

Hellstrom-Lindahl E, Westermark P, Antoni G, Estrada S. In vitro binding of 3H-PIB to human amyloid deposits of different types. Amyloid. 2014; 21:21–27. [PubMed: 24286359]

Herrmann N, Lanctot KL, Khan LR. The role of norepinephrine in the behavioral and psychological symptoms of dementia. J Neuropsychiatry Clin Neurosci. 2004; 16:261–276. [PubMed: 15377733]

Jameson LP, Smith NW, Dzyuba SV. Dye-binding assays for evaluation of the effects of small molecule inhibitors. ACS Chem Neurosci. 2012; 3:807–819. [PubMed: 23173064]

Klimek V, Stockmeier C, Overholser J, Meltzer HY, Kalka HY, Dilley G, Ordway GA. Reduced levels of norepinephrine transporters in the locus coeruleus in major depression. J Neurosci. 1997; 17:8451–8458. [PubMed: 9334417]

Klunk WE, Engler H, Nordberg A, Wang Y, Blomqvist G, Holt DP, Bergstrom M, Savitcheva I, Huang GF, Estrada S, Ausen B, Debnath ML, Barletta J, Price JC, Sandell J, Lopresti BJ, Wall A, Koivisto P, Antoni G, Mathis CA, Langstrom B. Imaging brain amyloid in Alzheimers disease with Pittsburgh compound-B. Ann Neurol. 2004; 55:306–319. [PubMed: 14991808]

Kung, HF., Kung, MP., Zhuang, ZP. Stilbene derivatives and their use for binding and imaging amyloid plaques. WO. 018070. 2003.

Logan J, Wang GJ, Telang F, Fowler JS, Alexoff D, Zabroski J, Jayne M, Hubbard B, King P, Carter P, Shea C, Xu Y, Muench L, Schlyer D, Learned-Coughlin S, Cosson V, Volkow ND, Ding YS.

Imaging the norepinephrine transporter in humans with (S,S)-[11C]O-methyl reboxetine and PET: Problems and progress. Nucl Med Biol. 2007; 34:667–679. [PubMed: 17707807]

Mathis CA, Mason NS, Lopresti BJ, Klunk WE. Development of positron emission tomography b-amylloid plaque imaging agents. Semin Nucl Med. 2012; 42:423–432. [PubMed: 23026364]

Mathis C, Wang Y, Holt DP, Huang GF, Debnath ML, Klunk WE. Synthesis and evaluation of 11C-labeled 6-substituted 2-arylbenzothiazoles as amyloid imaging agents. J Med Chem. 2003; 46:2749–2755.

Matsumura K, Ono M, Hayashi S, Kimura H, Okamoto Y, Ihara M, Takahashi R, Mori H, Saji H. Phenyldiazenyl benzothiazole derivatives as probes for in vivo imaging of neurofibrillary tangles in Alzheimer's disease brains. Med Chem Commun. 2011; 2:596–600.

Mirbolooki MR, Constantinescu CC, Pan ML, Mukherjee J. Quantitative assessment of brown adipose tissue metabolic activity and volume using 18F-FDG PET/CT and β3-adrenergic receptor activation. EJNMMI Res. 2011; 1:30. [PubMed: 22214183]

Mirbolooki MR, Constantinescu C, Pan ML, Mukherjee J. Targeting presynaptic norepinephrine transporter in brown adipose tissue: A novel imaging approach and potential treatment for diabetes and obesity. Synapse. 2013; 67:79–93. [PubMed: 23080264]

Mukherjee J, Shi B, Christian BT, Chattopadhyay S, Narayanan TK. ^{11}C-Fallypride: Radiosynthesis and preliminary evaluation of novel dopamine D2/D3 receptor PET radiotracer in nonhuman primate brain. Bioorg Med Chem. 2004; 12:95–102. [PubMed: 14697774]

Mukherjee M, Pan ML, Mirbolooki RM, Constantinescu C, Mukherjee J. 11C-TAZA, a new PET imaging agent for Aβ-amyloid plaques in the human brain. J Nucl Med. 2012; 53(suppl):1631.

Ni R, Gillberg P-G, Bergfors A, Marutle A, Nordberg A. Amyloid tracers detect multiple binding sites in Alzheimer's disease brain tissue. Brain. 2013; 136:2217–2227. [PubMed: 23757761]

Ono M, Wilson A, Nobrega J, Westaway D, Verhoeff P, Zhuang Z-P, Kung M-P, Kung HF. 11C-Labeled stilbene derivatives as Ab-aggregate-specific PET imaging agents for Alzheimer's disease. Nucl Med Biol. 2003; 30:656–671.

Okuyama C, Sakane N, Yoshida T, Shima K, Kurosawa H, Kumamoto K, Ushijima Y, Nishimura T. (123)I- or (125)I-metaiodobenzylguanidine visualization of brown adipose tissue. J Nucl Med. 2002; 43:1234–1240. [PubMed: 12215564]

Raniga P, Bourgeat P, Fripp J, Acosta O, Villemagne V, Rowe C, Masters CL, Jones G, O'Keefe G, Salvado O, Ourselin S. Automated 11C-PIB standardized uptake value ratio. Acad Radiol. 2008; 15:1376–1389. [PubMed: 18995189]

Rinne JO, Brooks DJ, Rossor MN, Fox NC, Bullock R, Klunk WE, Mathis CA, Belnnow K, Barakos J, Okello AA, Rodriguez Martinez de Liano S, Liu E, Koller M, Gregg KM, Schen D, Black R, Grundman M. ^{11}C-PiB PET assessment of change in fibrillar amyloid-beta load in patients with Alzheimer's disease treated with bapineuzumab; a phase 2, double-blind, placebo-controlled, ascending-dose study. Lancet Neurol. 2010; 9:363–372. [PubMed: 20189881]

Salloway S, Sperling R, Fox NC, Blennow K, Klunk W, Raskid M, Sabbagh M, Honig LS, Porsteinsson AP, Ferris S, Reichert M, Ketter N, Nejadnik B, Guenzler V, Miloslavsky M, Wang D, Lu Y, Lull J, Tudor IC, Liu E, Grundman M, Yuen E, Black R, Brashear HR. Two phase 3 trials of bapineuzumab in mild-to-moderate Alzheimer's disease. New Engl J Med. 2014; 370:322–333. [PubMed: 24450891]

Schenk D, Barbour R, Dunn W, Gordon G, Grajeda H, Guido T, Hu K, Huang J, Johnson-Wood K, Khan K, Kholodenko D, Lee M, Liao Z, Lieberburg I, Motter R, Mutter L, Soriano F, Shopp G, Vasquez N, Vandevert C, Walker S, Woquilis M, Yednock T, Games D, Seubert P. Immunization with amyloid-beta attenuates Alzheimer's disease like pathology in the PDAPP mouse. Nature. 1999; 402:537–540. [PubMed: 10591214]

Schweinhardt P, Fransson P, Olson L, Spenger C, Andersson JL. A template for spatial normalisation of MR images of the rat brain. J Neurosci Methods. 2003; 129:105–113. [PubMed: 14511814]

Shao X, Hoareau R, Hockley BG, Tluczek LJM, Henderson BD, Scott PJH. Highlighting the versatility of the Tracerlab synthesis modules. Part 2: Fully automated production of [^{11}C]-labeled radiopharmaceuticals using a Tracerlab FXC-Pro. J Label Compd Radiopharm. 2011; 54:819–838.

Smith HR, Beveridge TJ, Porrino LJ. Distribution of norepinephrine transporters in the non-human primate brain. Neuroscience. 2006; 138:703–714. [PubMed: 16427744]

Smith EL, Brown AS, Adjaye-Mensah E, Wilson JN. Probing the functional limits of the norepinephrine transporter with self-reporting, fluorescent stilbazonium dimers. Org Biomol Chem. 2012; 10:1493–1496. [PubMed: 22234608]

Snellman A, Lopez-Picon FR, Rokka J, Salmona M, Forloni G, Scheinin M, Solin O, Rinne JO, Haaparanta-Solin M. Longitudinal amyloid imaging in mouse brain with 11C-PIB: Comparison of APP23, Tg2576, and Appswe-PS1dE9 mouse models of Alzheimer's disease. J Nucl Med. 2013; 54:1434–1441. [PubMed: 23833271]

Spencer TJ, Biederman J, Wilens TE, Faraone SV. Novel treatments for attentiondeficit/hyperactivity disorder in children. J Clin Psychiatry. 2002; 63:16–22.

Stephenson KA, Chandra R, Zhuang Z-P, Hou C, Oya S, Kung M-P, Kung HF. Fluoropegylated (FPEG) imaging agents targeting Ab aggregates. Bioconjug Chem. 2007; 18:238–246. [PubMed: 17226978]

Streby KA, Shah N, Ranalli MA, Kunkler A, Cripe TP. Nothin but NET: A review of norepinephrine transporter expression and efficacy of 131I-mIBG therapy. Pediatr Blood Cancer. 2015; 62:5–11. [PubMed: 25175627]

Tu P, Fu H, Cui M. Compounds for imaging amyloid-β deposits in an Alzheimer's brain: A patent review. Expert Opin Ther Patents. 2015; 25:413–423.

Vandenberghe R, Van Laere K, Ivanoiu A, Salmon E, Bastin C, Triau E, Hasselbalch S, Law I, Andersen A, Korner A, Minthon L, Garraux G, Nelissen N, Bormans G, Buckley C, Owenius R, Thurfjell L, Farrar G, Brooks DJ. 18F-Flutemetamol amyloid imaging in Alzheimer's disease and mild cognitive impairment-A phase 2 trial. Ann Neurology. 2010; 68:319–329.

Villemagne VL, Ong K, Mulligan RS, Holl G, Pejoska S, Jones G, O'Keefe G. Amyloid imaging with 18F-florbetaben in Alzheimers disease and other dementias. J Nucl Med. 2011; 52:1210–1217. [PubMed: 21764791]

Verhoeff NP. Amyloid imaging in vivo: Implications for Alzheimer's disease management. Expert Opin Med Diagn. 2007; 1:337–349. [PubMed: 23489354]

Weiner MW, Veitch DP, Aisen PS, Beckett LA, Cairns NJ, Cedearbaum J, Donohue MC, Green RC, Harvey D, Jack CR Jr, Jagust W, Morris JC, Petersen RC, Saykin AJ, Shaw L, Thompson PM, Toga AW, Trojanowski JQ. Impact of the Alzheimer's disease neuroimaging initiative, 2004–2014. Alzheimers Dement. 2015; 11:865–884. [PubMed: 26194320]

Wilson A, Garcia A, Chestakova A, Kung H, Houle S. A rapid one-step radiosynthesis of the β-amyloid imaging radiotracer N-methyl-[^{11}C]2-(40-methylaminophenyl)-6-hydroxybenzothiazole ([11C]-6-OH-BTA-1). J Label Compd Radiopharm. 2004; 47:679–682.

Zhang W, Oya S, Kung M-P, Hou C, Maier DL, Kung HF. F-18 stilbenes as PET imaging agents for detecting b-amyloid plaques in the brain. J Med Chem. 2005; 48:5980–5988. [PubMed: 16162001]

Zimmer ER, Leuzy A, Gauthier S, Rosa-Neto P. Developments in Tau PET imaging. Can J Neurol Sci. 2014; 41:547–553. [PubMed: 25424608]

Zhu L, Ploessl K, Kung HK. PET/SPECT imaging agents for neurodegenerative diseases. Chem Soc Rev. 2014; 43:6683–6691. [PubMed: 24676152]

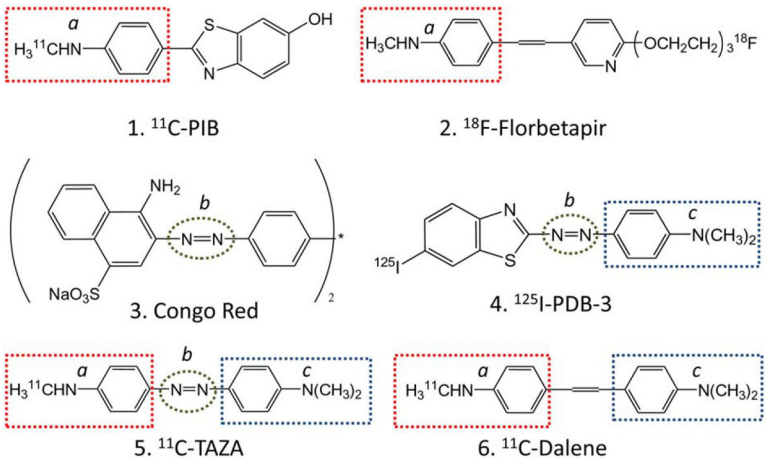

Fig. 1.

Chemical structures of Aβ binding ligands: **1**. [^{11}C]PIB; **2**. [^{18}F]Florbetapir; **3**. Congo red; **4**. [^{125}I]PDB; **5**. [^{11}C]TAZA; **6**. [^{11}C]Dalene. The common "*N*-methylaminophenyl"structure is shown in red dotted boxes for the four PET radiotracers. The common "azo" feature between Congo red, PDB and TAZA is shown in dotted green ovals and the common "*N*,*N*-dimethylaminophenyl" feature between PDB, TAZA and Dalene is shown in blue dotted boxes.

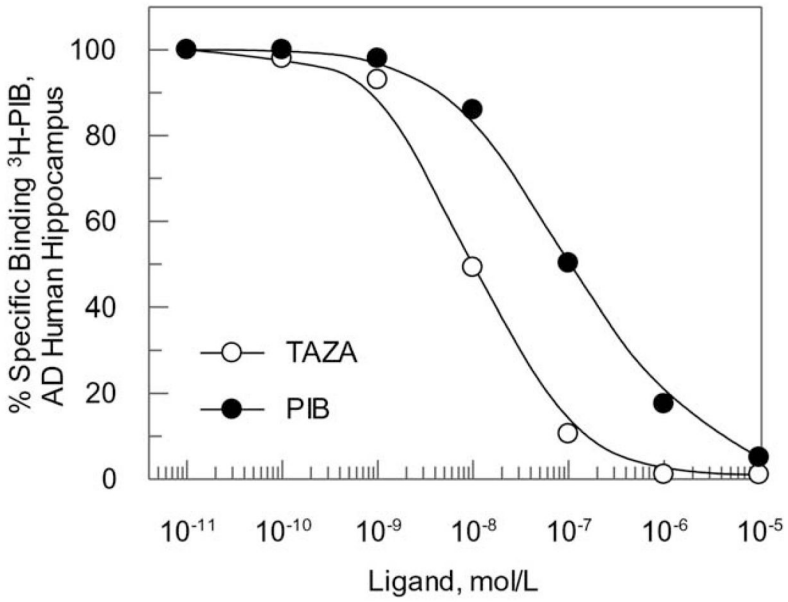

Fig. 2.

Binding affinity: inhibition curves of [^{3}H]PIB-labeled Aβ plaques in postmortem human brain hippocampal homogenate by TAZA and PIB (average of two measurements). The measured IC50 values were TAZA= 1.28 nM and PIB =10 nM and calculated K_i values were TAZA= 0.84 nM and PIB= 6.67 nM.

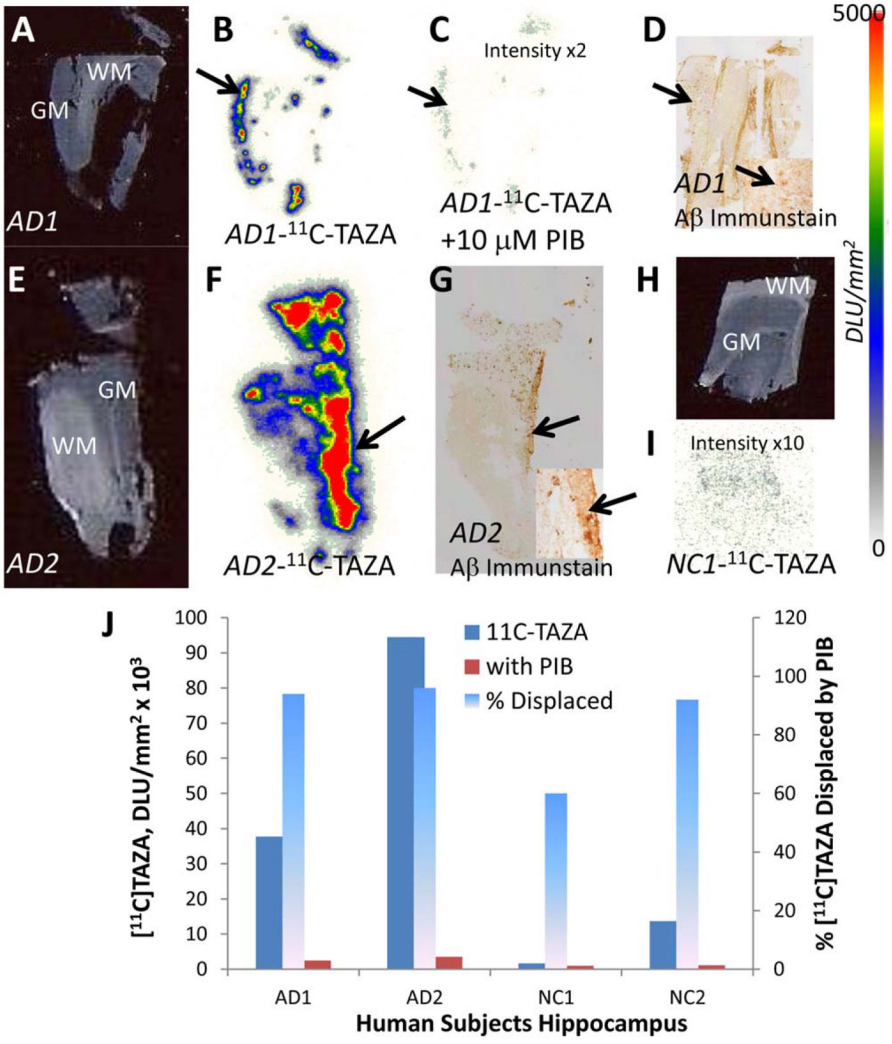

Fig. 3.

Postmortem human brain autoradiography [^{11}C]TAZA: (**A**,**E**) Human postmortem AD brain hippocampus sections (7 μm) showing gray matter (GM) and white matter (WM); (**B**,**F**). Binding of [^{11}C]TAZA to Aβ plaques (shown by arrows) in AD1 and AD2 hippocampus sections shown in (A,E); (C) [^{11}C]TAZA in AD1 displaced by 10 μM PIB and normal brain tissue; (**D**,**G**) Aβ plaques immunostained (shown by arrow) in the GM (inset ×10 magnification); (**H**) Human postmortem normal control brain hippocampus sections (7 μm) showing gray matter (GM) and white matter (WM); (**I**) Little binding of [^{11}C]TAZA seen in (H) (intensity ×10); (**J**) Plot showing [^{11}C]TAZA binding in GM of the four subjects in the absence and presence of 10 μM PIB and percent displacement by PIB.

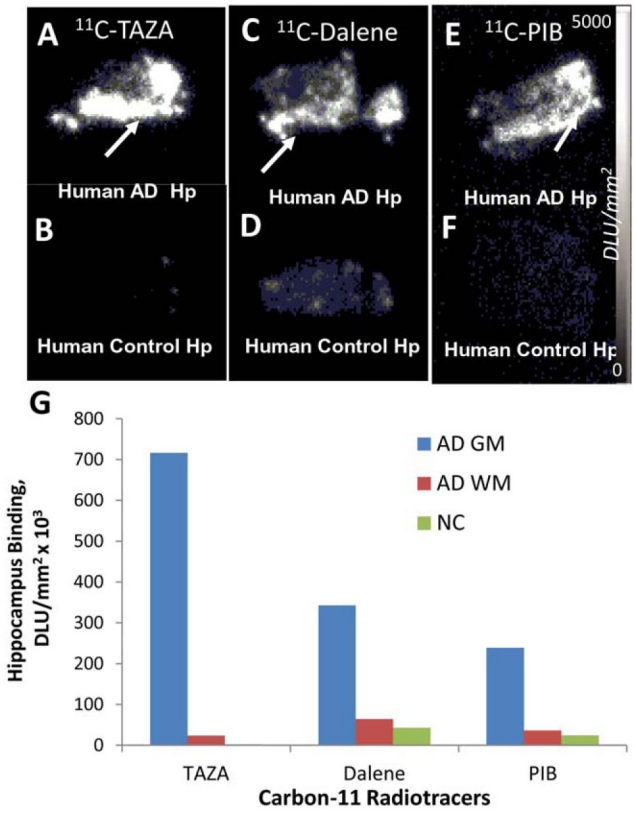

Fig. 4.

Comparison of [^{11}C]TAZA with [^{11}C]PIB and [^{11}C]Dalene: (**A**,**B**) Postmortem human AD and NC hippocampus showing binding of [^{11}C]TAZA to Aβ plaques (arrow); (**C**,**D**) Postmortem human AD and NC hippocampus showing binding of [^{11}C]Dalene to Aβ plaques (arrow); (**E**,**F**) Postmortem human AD and NC hippocampus showing binding of [^{11}C]PIB to Aβ plaques (arrow); (**G**) Plot comparing GM and WM in AD subject and NC for the three radiotracers.

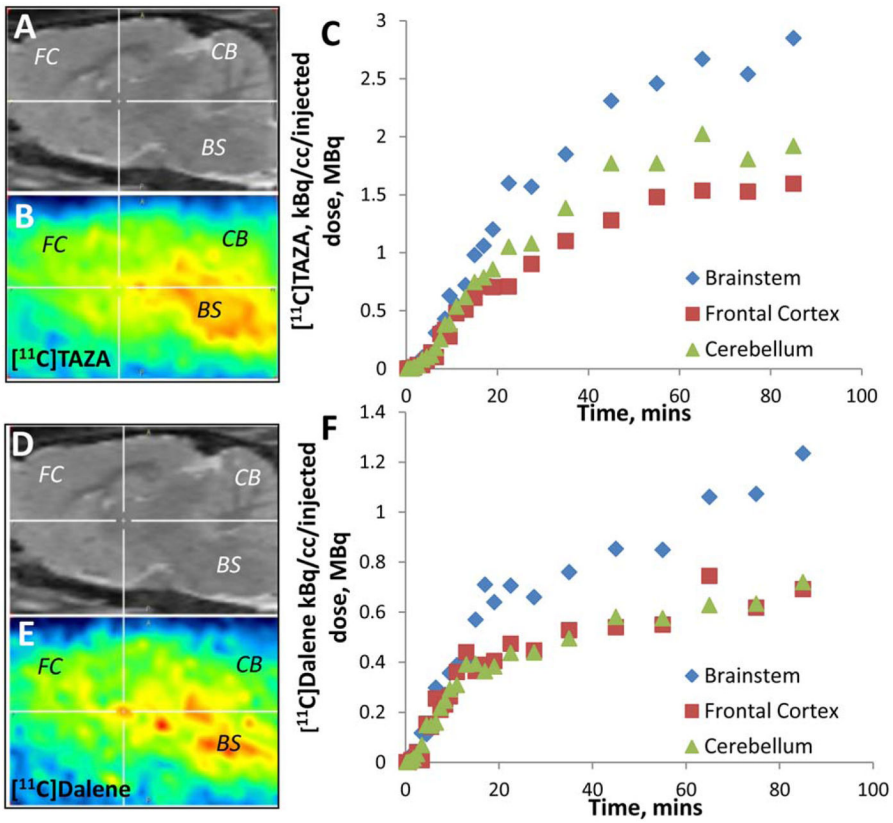

Fig. 5.

Brain PET in Normal Rats: Sagittal sections (1.2 mm with respect to midline) through the rat brain from both [^{11}C]TAZA (injected with 90 MBq) and ^{11}C-Dalene (injected with 102 MBq). PET images are from baseline condition and frames were averaged >20–90 min. (**B**, **E**) Shows PET images associated with the MR template (**A**, **D**). The cross hair is positioned at 2.6 mm (A–P) and 5.7 mm (D–V) with respect to bregma. Time activity curves of [^{11}C]TAZA (C), and ^{11}C-Dalene (**F**) for brainstem (BS), frontal cortex (FC) and cerebellum (CB) regions are shown. [^{11}C]TAZA approached a plateau in the CB approximately 50 min postinjection while [^{11}C]Dalene approached a plateau in the CB approximately 40 min postinjection.

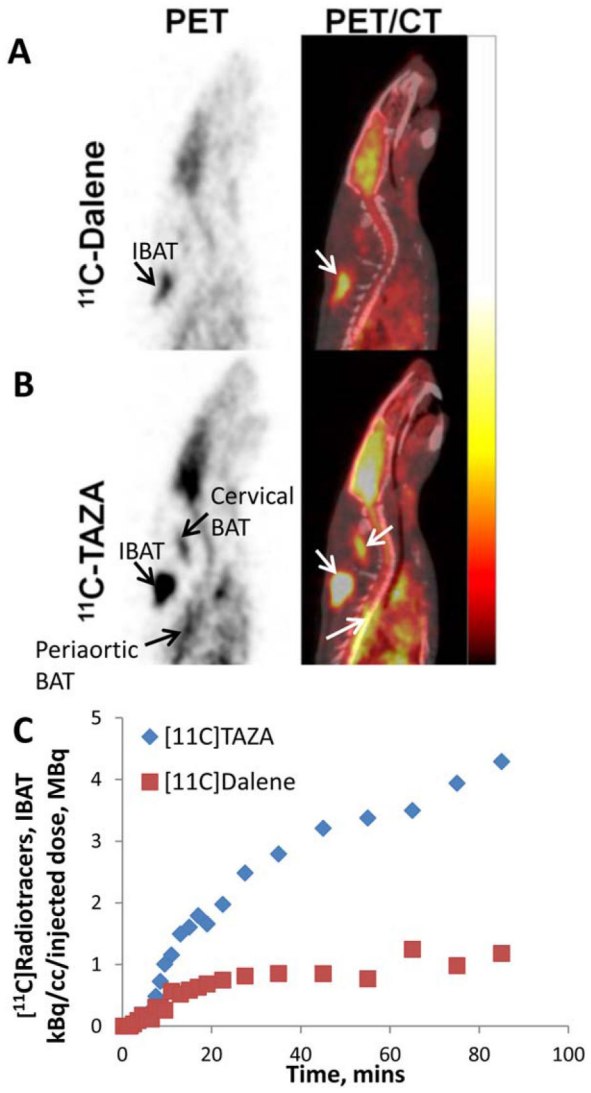

Fig. 6.

Whole body PET/CT in normal rats: Whole body PET (left), and coregistered PET/CT (right) sagittal views of rats showing [^{11}C]Dalene (**A**) and [^{11}C]TAZA (**B**) average uptake >90 min postinjection. (A) Localization of [^{11}C]Dalene in IBAT is clearly visualized in both the PET and PET/CT images; (B) Localization of [^{11}C]TAZA in IBAT, cervical BAT and periaortic BAT is clearly visualized in both the PET and PET/CT images; (**C**) Time-activity curves of [^{11}C]Dalene and [^{11}C]TAZA in IBAT showing a plateauing effect for [^{11}C]Dalene in 30 min while [^{11}C]TAZA continues to rise reaching an approximate plateau in 90 min.

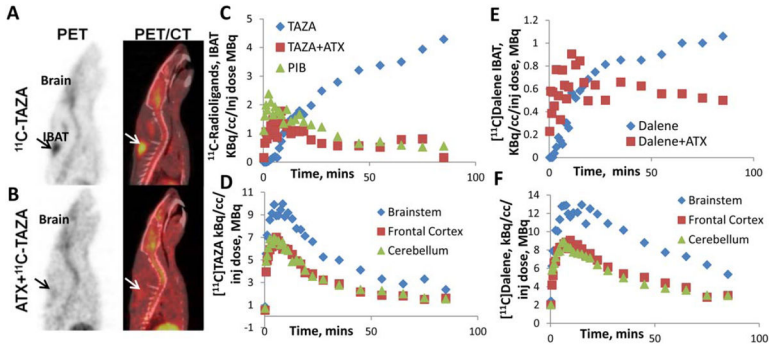

Fig. 7.

Atomoxetine effects: (**A**,**B**) Sagittal views of PET (left) and PET/CT (right) images show [^{11}C]TAZA uptake in IBAT >90 min after the injection. (B) Atomoxetine (2 mg/kg intravenous, 2 min prior to [^{11}C]TAZA, 49 MBq) reduced binding to IBAT significantly. (**C**) IBAT time activity curves for [^{11}C]TAZA with and without atomoxetine, compared with [^{11}C]PIB showing rapid uptake and clearance of [^{11}C]TAZA in the presence of atomoxetine. (**D**) Brain time activity curves for [^{11}C]TAZA with preadministration of atomoxetine showing rapid uptake and clearance of [^{11}C]TAZA from all brain regions. (**E**) IBAT time activity curves for [^{11}C]Dalene without and with atomoxetine (1 mg/kg intravenous, 17 min prior to [^{11}C]Dalene, 37 MBq). IBAT activity was reduced significantly. (**F**) Brain time activity curves for [^{11}C]Dalene with preadministration of atomoxetine showing rapid uptake and clearance of [^{11}C]Dalene from all brain regions.

TABLE I

Binding affinity of compounds

Compounds	IC_{50}/K_i, nM	Binding affinity Relative to PIB	Primary target
PIB	K_d = 3.77[a]; IC_{50}=3.84[b]	1	Aβ plaques
	K_i =0.87[c]		
	$IC_{50}=10/K_i$ =6.67[d]		
TAZA	IC_{50}=1.28[d]	7.81[g]	Aβ plaques
	K_i =0.84[d]	4.49[h]	
Dalene (Compound #25 in reference)	K_i =15.2[e]	(0.21)[i]	Aβ plaques
Florbetapir	K_i =2.87[c]	0.30[j]	Aβ plaques
Florbetaben	K_i =2.22[c]	0.39[j]	Aβ plaques
Flutmetamol	K_i =0.74[c]	1.18[j]	Aβ plaques
AZD4694 (NAV4694)	K_i =2.3[c]	0.35[j]	Aβ plaques
PDB-3 Phenyldiazenyl benzothiazole[g]	K_i = 8.24[f]	(9.85)[i]	Aβ plaques Tau
	K_i = 0.48[k]		

[a] Human AD brain homogenate kDa using ^{3}H-PIB (Fodero-Tavoletti *et al.*, 2007).

[b] Human AD frontal cortex IC_{50} using ^{3}H-PIB (Hellstrom-Lindahl *et al.*, 2014).

[c] K_i AD brain homogenates using ^{18}F-florbetapir (Choi *et al.*, 2009).

[d] This work, human hippocampal homogenate using ^{3}H-PIB.

[e] K_i using ^{125}I-TZDM (Kung *et al.*, 2003; Compound #25 in Patent).

[f] K_i measured using thioflavin (Matsumura *et al.*, 2011).

[g] Compared to PIB IC_{50}= 10 nM, this work.

[h] Compared to kd[a]= 3.77 nM in AD brain homogenate using ^{3}H-PIB (Fodero-Tavoletti *et al.*, 2007).

[i] Compared to affinity measures of SB-13 in the same assay.

[j] Compared to K_i = 0.87 nM in AD brain homogenates using ^{18}F-florbetapir (Choi *et al.*, 2009).

[k] K_i measured using thioflavin-S for Tau with Aβ/Tau ratio of >17 (Matsumura *et al.*, 2011).

TABLE II

Postmortem human hippocampus autoradiography

Subjects[a]	Aβ plaque stage and tangle stage	[11C]TAZA GM/WM	[11C]Dalene GM/WM	[11C]PIB GM/WM
AD1	Stage C	19.6	3.68	5.47
Female, 89 yrs	Stage 6			
AD2	Stage C	30.5	5.34	7.48
Female, 93 yrs	Stage 6			
NC1	Stage A	~1	~1	~1
Male, 90 yrs	Stage 3			
NC2	Stage A	Local hot spots	Local hot spots in	Local hot spots in
Female, 91 yrs	Stage 2	in grey matter (≥5)	grey matter (~2)	grey matter (~2)

[a]Postmortem interval (PMI) ranged from 2.6 to 5.8; Neuropsychological deficits (NPD) confirmed of Alzheimer's disease (AD) and normal controls (NC). Frozen tissue (at −80°C) was sectioned in 7 μm thickness at −20°C and used for the study. GM =Gray matter; WM =White matter.

TABLE III

In vivo pet measures of [^{11}C]radiotracers in rats

	Brain, %injected dose/cc						IBAT %Injected dose/cc	
Radiotracer	**Brain-stem**	**Brain-stem +ATX**	**Frontal Cortex**	**Frontal Cortex +ATX**	**Cerebellum**	**Cerebellum +ATX**	**Baseline**	**+ATX**
[^{11}C]TAZA								
4.5 min[a]	0.013	0.990	0.007	0.627	0.010	0.695	0.015	0.148
85 min[b]	0.285	0.237	0.160	0.160	0.192	0.154	0.429	0.016
Ratio[c]	*0.05*	*4.2*	*0.04*	*3.92*	*0.05*	*4.51*	*0.04*	*9.25*
[^{11}C]Dalene								
4.5 min[a]	0.011	1.13	0.015	0.828	0.015	0.788	0.018	0.054
85 min[b]	0.124	0.534	0.069	0.304	0.072	0.304	0.118	0.050
Ratio[c]	*0.09*	*2.12*	*0.22*	*2.72*	*0.21*	*2.59*	*0.15*	*1.08*
[^{11}C]PIB								
4.5 min[a]	0.165	NA	0.714	NA	0.823	NA	0.165	NA
85 min[b]	0.056		0.045		0.124		0.056	
Ratio[c,d]	*2.95*		*15.9*		*6.64*		*2.95*	

[a]Initial time of maximal uptake of radiotracers.

[b]End of scan time.

[c]Ratio= uptake at 4.5 min/uptake at 85 min.

[d]Reported brain [^{11}C]PIB 2 min/30 min percent injected dose/g in mice ratio= 11 (Mathis *et al.*, 2012). ATX= Atomoxetine; NA= Not available.